scientific reports

Check for updates

OPEN

A high-performance extracellular field potential analyzer for iPSC-derived cardiomyocytes

Nidhi Patel[1,4], Alex Shen[1,4], Yuko Wada[1], Marcia Blair[1], Devyn Mitchell[1], Loren Vanags[1], Suah Woo[1], Matthew Ku[1], Kundivy Dauda[1], William Morris[1], Minjoo Yang[1], Björn C. Knollmann[1,2], Joe-Elie Salem[1,3], Andrew M. Glazer[1✉] & Brett M. Kroncke[1✉]

Induced pluripotent stem cell-derived cardiomyocytes (iPSC-CMs) have emerged as a pivotal model for research. Specialized devices can generate Extracellular Field Potential (EFP) measurements from these cells, analogous to the ventricular complex of the electrocardiogram. However, electrophysiological analysis can be complex and requires specialized expertise, posing a barrier to broader adoption in non-specialized labs. We present the EFP-Analyzer (EFPA), a semi-automized analyzer for EFP traces, which identifies and averages beats, identifies landmarks, and calculates intervals. We demonstrate an analysis of 358 EFP traces from 22 patient-derived lines. We analyzed spontaneously beating iPSC-CMs and optically paced iPSC-CMs through channelrhodopsin. We developed stringent quality criteria and measured EFP intervals, including Field Potential Duration (FPD). We further analyzed the usability and data replicability of EFPA through an inter-intra observer analysis. Correlation coefficient for inter-reader tangent and threshold measurements for these FPD ranged between r: 0.93–1.00. Bland–Altman plots comparing inter observer results for spontaneously beating and paced iPSC-CMs showed 95% limits of agreement (– 13.6 to 19.4 ms and – 13.2 to 15.3 ms, respectively). EFPA could accurately detect FPD prolongation due to drug (moxifloxacin) or pathogenic loss of function mutations (CACNA1C N639T). This program and instructions are available for download at https://github.com/kroncke-lab/EFPA.

Keywords In Vitro, Ion channels, Model evaluation, Pharmacology, Stem Cells, Translational Medicine

Since their discovery in 2006[1], induced pluripotent stem cells (iPSCs) have become a transformative tool for modeling cell behavior, drug response, and disease[2]. A number of groups have developed methods for differentiating iPSCs into cardiomyocytes (CMs)[3]. These induced pluripotent stem cell derived cardiomyocytes (iPSC-CMs) are an emerging model for the study of drug safety screening, in particular for detecting drugs that prolong the cardiac action potential duration[4,5]. Cardiovascular liability has been a major reason for clinical trials abandonment in the 2000s (non-clinical = 27%, phase I-III = 21%, post approval = 45%)[6]. In particular, to prevent torsadogenic drugs from entering the market, there have been extensive efforts to deploy preclinical assays to evaluate hERG inhibition as a key determinant of proarrhythmia[7]. IPSC-CMs have also been used to study genetic background variability in electrocardiographic properties and drug response[8]. In addition, CRISPR enables variant-specific disease modeling in iPSC-CMs through targeted introduction of candidate variants. For example, *KCNH2* T983I iPSC-CMs had decreased I_{Kr} density, supporting the classification of T983I as a Long QT type 2 variant[9]. In addition, *CACNA1C* N639T iPSC-CMs had increased FPD, supporting its classification as a Long QT type 8 variant[10]. Advancements in optogenetic methods have allowed for the expression of channelrhodopsin, a light activated ion channel, in iPSC-CMs to enable optical pacing[11]. More accurate investigations of cardiac function and pharmacological effects make it possible to precisely and non-invasively control cardiomyocyte activity. Although iPSC-CMs are thought to represent a relatively immature state of cardiac differentiation, recent methods have resulted in improved ventricular cardiomyocyte differentiation, successfully profiling all major cardiac currents in iPSC-CMs[12]. The Extracellular Field Potential (EFP) is

[1]Department of Medicine, Vanderbilt University School of Medicine, 2215 Garland Ave, Nashville, TN 37232, USA. [2]Department of Pharmacology, Vanderbilt University Medical Center, 2215 Garland Ave, Nashville, TN 37232, USA. [3]Department of Pharmacology Clinical Investigation Center, INSERM, Pitié-Salpêtrière University Hospital, Sorbonne Universite, Paris-Est 47 Boulevard de L'Hopital, CIC-1901 Paris, France. [4]Nidhi Patel & Alex Shen are equal contributors to this work and are designated as co-first authors. ✉email: andrew.m.glazer@vumc.org; brett.kroncke@gmail.com

nature portfolio

1

generated by the movement of ions across the cell membrane during contraction, and is measured by adjacent electrodes[13]. EFP signatures directly represent a cardiomyocyte's beating pattern and could be considered analogous to the electrocardiogram (ECG). Previous literature defined the analogous time-based parameters as depolarization time (DT), repolarization time (RT), and maximum field potential duration (FPDmax).

ECG analysis software automation is widespread with extensive validation regarding consistency of these measurements[14]. The heart has large conduction distances and regions with distinct beating patterns, such as the atria, ventricles, and his-Purkinje complexes. In contrast, iPSC-CM monolayers are a relatively uniform substrate with small conduction distances. Although the EFP representation appears analogous to the ventricular complex (Depolarization and Repolarization) of the ECG (Fig. 1), relatively little work has demonstrated the consistency or reliability of EFP measurements, including intra and inter observer reliability. In addition, no standardized analysis tools have been made to analyze EFP morphology and parameters. Previous studies have adapted ECG analyzers such as LabChart designed for in vivo animal analysis, used software built-in to the devices, or used custom analysis methods without assessing reliability of these strategies[15–17].

We present the EFP-Analyzer (EFPA), a semi-automated software tool for analysis of EFP traces. We use the EFP-Analyzer to analyze a large dataset of 358 control EFPs from 22 control patients and provide guidelines for stringent quality criteria. We show that this tool is fast to use, and generates consistent, reliable measurements. We further validate the EFPA's ability to characterize iPSC-CM properties in two scenarios: measurements of Kv11.1 inhibition causing delayed cardiac repolarization, and characterization of a CACNA1C gain-of-function variant leading to slow $Ca_v1.2$ voltage-dependent inactivation and prolonged action potentials. The
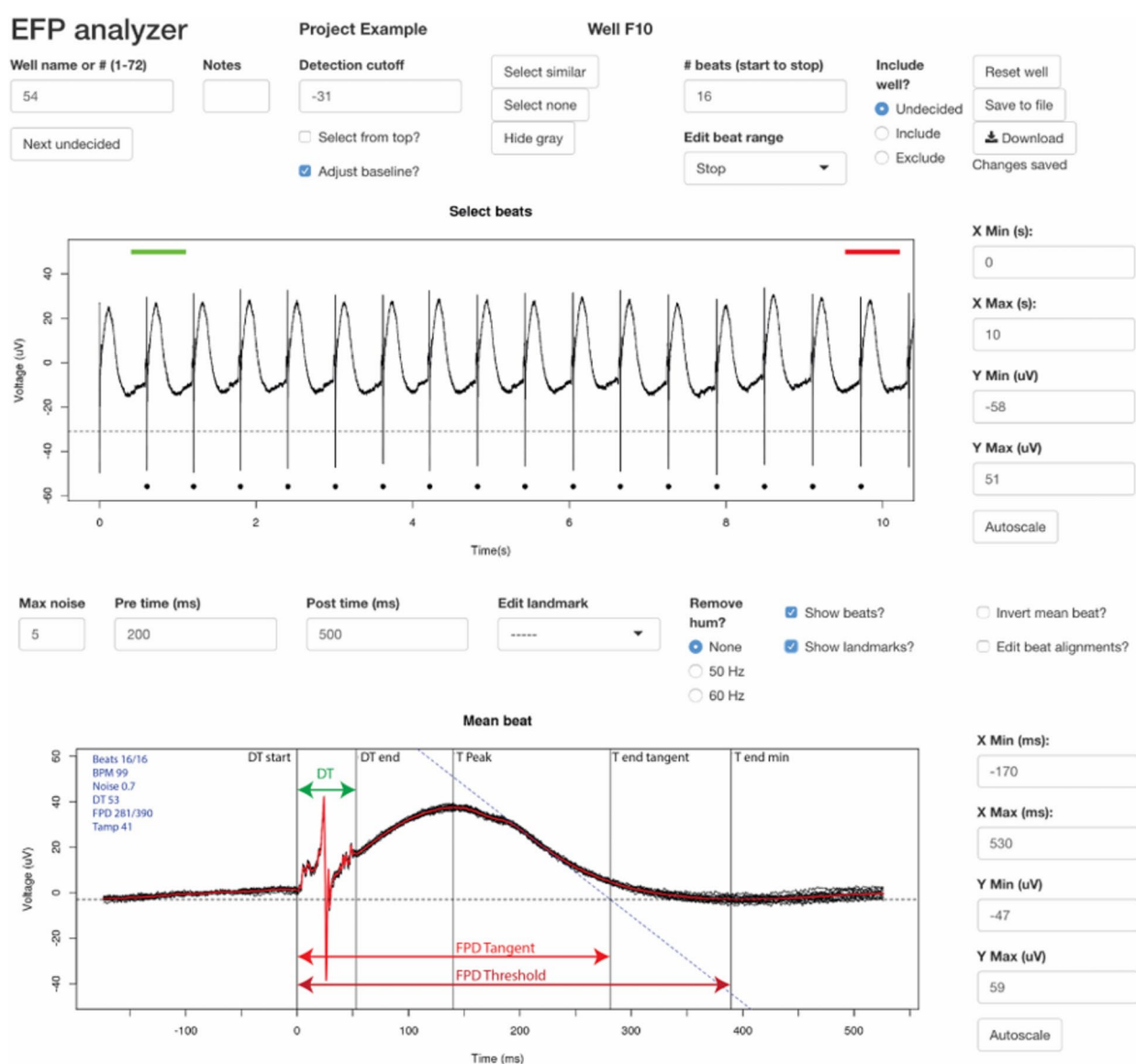

Fig. 1. EFP Analyzer Software User Interface. An EFP Analyzer tool with graphical and parameter input settings that shows the procedures for beat selection, landmark editing, and field potential duration (FPD) analysis.

EFPA successfully and accurately detect changes in FPDmax from QT prolonging drug (moxifloxacin) or loss of function mutation (CACNA1C N639T). This tool will help facilitate the use of EFPs in iPSC-CMs for drug screening and disease modeling.

Materials and methods

Generation of iPSC lines:

All experimental protocols were approved by Vanderbilt University Medical Center (VUMC). All experimental methods were carried out in accordance with VUMC Guidelines and regulations. Patient informed consent was obtained from all subjects and/or their legal guardian(s) under VUMC IRB #040,551. Eight female and seven male participants with no known congenital arrhythmia syndromes were chosen (Figure S1). Peripheral blood mononuclear cells were isolated from blood and reprogrammed into iPSCs using electroporation delivery (Neon system, ThermoFisher) of non-integrating episomal vectors (Epi5 Episomal iPSC Reprogramming Kit, ThermoFisher). Colonies exhibiting iPSC-like morphology were manually transferred to hES-grade Matrigel (Corning)-coated 24-well plates between days 14 and 30 post-electroporation. Individual colonies were then expanded for validation and line maintenance. Individual colonies were expanded for validation and line maintenance. Selected iPSCs were validated by staining with OCT4 (Cell Signaling, #2750), SSEA4 (DSHB, MC-813–70), SSEA3 (Millipore, MAB4303), and Tra1-60 (Millipore, MAB4360). All iPSC lines used in this study were karyotype normal (Genetics Associates, Nashville, TN).

Cardiomyocyte differentiation:

IPSC's were cultured in mTeSR media for 4–5 days to achieve ~ 80% confluency. Media was changed to cardiac differentiation medium: RPMI 1640 (11,875, Life Technologies), 2% B-27 minus insulin supplement (A1895601, Life Technologies), and 1% Penicillin–Streptomycin (Life Technologies). From days 0–2 the media was supplemented with 6 μM CHIR99021 (LC Laboratories), and from days 3–5 with 5 μM IWR-1 (Sigma). From days 13–19 metabolic selection medium was used: RPMI1640 without glucose (11,879, Life Technologies), 2% B-27 minus insulin supplement (A1895601, Life Technologies), and 1% Penicillin–Streptomycin (Life Technologies). For days 19 + cardiomyocyte media was used. Media was exchanged every other day. Selected iPSC-CM were validated by staining with alpha-actinin (Sigma) and myosin light chain-2 V (ProteinTech) (Figure S2). Optically paced cells were treated from days 28–30 with 6500 genome copies/cell of AAV1.CAG.hChR2(H134R)-mCherry. WPRE.SV40 (Addgene20938M) purchased from the University of Pennsylvania Vector Core. At day 30, 60,000 cardiomyocytes per well were replated into CardioExcyte96 sensor plates (Nanion) coated with 50 μl of 1:100 Matrigel, and cells were studied at day 38–42 post-differentiation.

Confocal microscopy:

Generated hiPSC lines were layered onto a cultrex stem cell qualified reduced growth factor basement membrane extract (cat# 3434–005-02 R&D systems Inc) coated 6-well plate with cover slips (cat#12–542-BP FisherBrand) in each well. 2 mL of 4% PFA (cat#28,906 Thermofisher) in PBS (cat#10,010–023 Gibco) were fixed for 30 min at room temperature. After fixation, cells were washed three times with PBS to remove residual PFA. Next, cells were permeabilized with 0.2% Triton X-100 (cat#T8787 Sigma) in PBS for 20 min at room temperature. Cells are then blocked with 2 mL blocking solution made of 5% BSA (cat#A3059-10G Sigma) and 0.05% Triton X-100 in PBS for 2 h at 4 °C. Primary antibodies against cardiomyocyte markers, Monoclonal Anti-α-Actinin antibody (Sigma, A7811-100UL) and Myosin Light Chain 2/MLC-2 V (ProteinTech 10,908-AP), were added with 500 μL of blocking solution to the cells and incubated overnight at 4 °C on a shaker. After incubation with primary antibodies, cells are washed three times with 0.05% Triton X-100/PBS for 5 min each. Secondary antibodies were then added with 500 μL of blocking solution and incubated for 4 h at overnight at 4 °C on a shaker. After secondary antibody incubation, cells were washed three times with 0.05% Triton X-100/ PBS for 5 min each. Next, 1 mL of Hoechst dye 2 ug/mL (cat#B1155 Sigma) in PBS was added to cells for nuclear counterstaining and incubated for 5 min at room temperature. After Hoechst dye incubation, cells were washed three times with PBS for 5 min each. Cells were then placed onto a glass slide (cat#12–550-433 Fisherbrand) with aqua hold 2 pen (Cat# 9804–02 Scientific Device) to seal slide, and then a cover slip was added with 50% glycerol (cat#17,904 Sigma) in PBS. The edges of the cover slip were sealed with nail polish and dry overnight at 4 °C. Stained slides were imaged on Zeiss LSM 710 confocal microscope.

EFP measurement:

EFP and impedance signals (Figure S3) were measured on the CardioExcyte96 (Nanion) 8–12 days after replating (day 38–42 post-differentiation). Cells were kept at 37 °C, 80% humidity, and 5% CO2. For optical pacing, a stimulating optical lid (Nanion) was used, which exposed all wells to 470 nm wavelength light. Cells were exposed at 1 Hz to 5 ms-long pulses of light at 30 mA power. 20–30 s sweeps were recorded at an acquisition rate of 0.1 ms. Optical pacing was chosen over traditional electrical pacing to eliminate electrical Fstimulation artifacts, ensuring cleaner and more accurate EFP signal recordings. Additionally, optical pacing provides precise, artifact-free activation of cardiomyocyte monolayers, enhancing the reliability of repolarization analysis. Raw EFP and impedance measurements were converted into tab-delimited files through conversion of the "seconds" column from raw reads into a base.txt, followed by third column appended to base.txt as a new column. All data was then combined into LabChartinput.txt.

EFP-analyzer analysis:

The user interface and analysis logic of the EFP Analyzer software are presented in Fig. 1. The user is first presented with a data input screen which allows the import of a tab delimited file containing time in seconds in column 1 and EFP measurements from multiple samples (wells) in columns 2 + . Alternatively, the user can

also load a previously analyzed project. Upon loading the input files and selecting initial settings, screen 2 is presented, which contains the main analysis. The top plot displays the entire sweep, from which beats can be selected automatically or manually for analysis. Beats are averaged and displayed in plot 2. Beats deviating from the mean beat by more than the noise cutoff are eliminated. Landmarks for the DT complex, the T peak, the T_{end} tangent point, and the T_{end} threshold point are selected automatically or manually (Fig. 1). The user can navigate between samples and choose which samples to include or exclude. Measurements and plots can be downloaded to the user's computer as a series of .csv and .pdf files. Additional EFP Analyzer features are described in the GitHub README.

Analysis of control EFPs:

From our initial set of 25 control lines, wells were subjected to quality control (QC) on a per-well basis. This led to the exclusion of nearly every well from 3 of the lines, therefore these three lines were excluded from the study. After QC, there were 14 AAV-treated and 8 non-AAV-treated lines (Figure S4). All EFPs were classified by morphology into one of 3 categories: standard, low amplitude, and biphasic (Fig. 2). Low amplitude traces were defined as traces with a repolarization wave maximal amplitude (T peak) less than 10 uV. Biphasic traces were defined as those having two distinct repolarization waves in opposite directions, each later than 50 ms after the beginning of depolarization. Although there was variation in the morphology of depolarization waves, especially for spontaneously beating cells, this variation was not specifically used for classifying EFP morphologies. The mean beat was defined by the average of the beginning of the depolarization time to the end of the T wave from selected beats. Irregular traces were excluded, as standard, repeatable beats were preferred to avoid the complexity of median representative beat analysis. Irregular or ambiguous trace were classified manually, focusing on key characteristics that deviated from expected EFP morphologies: high noise, high baseline artifact, inconsistent morphology or intervals across beats. Optically paced traces not at 1 beat per second were excluded. Each EFP was then measured with the EFP Analyzer tool as described above.

Analysis of EFPs after exposure to an IKr-Blocker or to pathogenic genetic variant in CACNA1C:

Moxifloxacin, a hERG channel blocker[18], was applied to a subset of participant generated iPSC-CMs without a known congenital arrhythmogenic genetic background, in increasing doses (10 uM, 30 uM, 100 uM, 300 uM) at 1-h intervals. The iPSC lines heterozygous for CACNA1C N639T were generated as previously described[10,19]. Statistical analyses were performed in R (version 4.1.2).

Results
Description of EFP-analyzer software tool

We developed the EFP-Analyzer software tool, a Shiny-based interactive tool, available for download at https://github.com/kroncke-lab/EFPA. The GitHub README page provides clear, detailed instructions to guide users through installation, ensuring compatibility across various operating systems, including Microsoft Windows and macOS. The tool comprises two separate pages: a data load screen and a data analysis screen (Fig. 1). In the data load screen, users upload a dataset of EFP signal versus time, formatted in a comma separated values (.csv) file, and select analysis parameters. In the data analysis screen, beats are selected and averaged, landmarks are placed and intervals are calculated. The philosophy of the program is that it is "semi-automated" and
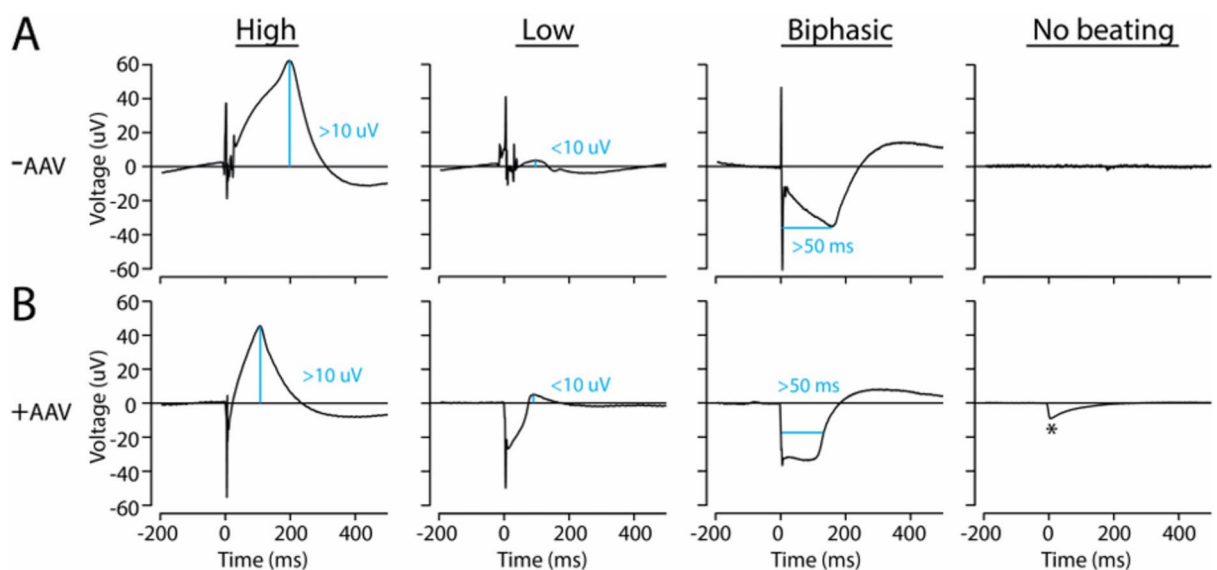

Fig. 2. EFP Morphologies for Spontaneously Beating and Paced Cells. (**A**) Example EFP morphologies for spontaneously beating cells (-AAV). (**B**) Example EFP morphologies for paced cells (+ AAV). * Indicates a light pacing artifact.

landmarks resemble to the one used to evaluate ventricular depolarization (QRS) and repolarization processes (QT) in human ECG. Therefore, these parameters are named DT and FPD. The program performs these tasks automatically once a new well is loaded. Users can modify the beat location and landmark placement.

Analysis of 22 iPSC-CM lines

We applied the EFP-Analyzer to EFPs generated from the CardioExcyte96, a 96-well plate format EFP generator from Nanion. We evaluated iPSC-CM lines derived from individuals without apparent genetic arrhythmia disorders. From the recorded 25 patient lines, we screened a total of 1280 traces (30 s per trace). Due to patient-specific factors including limited initial blood samples and variation in differentiation efficiency, there was a range in the number of traces recorded (8–150). Additional factors that contribute to this variability include variations in cell handling, plating effectiveness, and in-vitro survival rates.

The traces were categorized into spontaneous beating traces and those treated with AAV-ChR and optically paced. From an initial dataset of 708 spontaneous and 572 optically paced traces, wells that were not beating or irregularly beating were initially excluded for non-beating or irregular wells, leaving 430 spontaneous traces and 124 AAV traces. These were further excluded for small-amplitude and biphasic repolarization waves, leaving 303 spontaneous traces and 55 AAV traces from 22 patient lines (Figure S4). To assess the EFP-Analyzer's consistency in measuring FPDmax on EFP traces, we classified EFP morphology into three categories: standard, low amplitude, and biphasic (Fig. 2).

The consistency and bias, defined as the mean difference between repeat measurements, were evaluated as a function of trace morphology. EFPs with standard morphology exhibited the highest measurement reproducibility, while EFPs with low amplitude or biphasic morphology were poorly reproducible and highly scattered (Table 1). Subsequent analyses focused on EFPs with standard morphology, which included 303 spontaneous traces (303/708, 43%) and 55 high-quality AAV-ChR traces (55/572, 9.6%), forming the main dataset. The difference in the percentage of standard traces between spontaneous standard (43%) and paced AAV-ChR (9.6%) traces is primarily due to our strict exclusion criteria for paced cells. In addition to the other QC criteria, paced traces that did not have a consistent 1 Hz beating rate were removed from the study.

A random selection of 260 paced and 430 unpaced traces (stratified by EFP repolarization morphology) were measured by an expert (AG), who helped create the program and had an extensive history of analyzing iPSC-CM EFP traces, and by a novice (YW), who had a training session of 10 min in how to analyze the data and use the tool (~ 10 EFP test measurements) (Figure S5). All traces were measured by an expert analyzer (AG) using two methods: a simple threshold method and a tangent method, both based on different DT approaches reflective of human ECG measurement techniques (Table 1). The differences in FPD between spontaneous and paced EFPs, when measured using the threshold method, followed the same trend as those measured using the tangent method (Table 1). Among spontaneously beating and paced cells, FPD was not significantly correlated with RR interval (Spearman rho = 0.183, p = 0.135 for spontaneous; rho = -0.165, p = 0.147 for paced cells; Figure S6). FPDs assessed by the tangent method were shorter and had a lower dispersion than FPDs assessed by the threshold method in AAV-treated cells (283.7 ± 54.2 vs. 442.9 ± 109.2, p: < 0.001, respectively, Table 1). Bland–Altman plots for FPD (tangent method) measured by two readers showed 95% limits of agreement ranging from -13.6 to 19.4 ms for spontaneous traces and -13.2 to 15.3 ms for paced traces (Fig. 3 and Table 2). For intra-reader measurements, Bland–Altman plots showed 95% limits of agreement ranging from -22.6 to 21.5 ms for spontaneous traces and -17.4 to 17.0 ms for paced traces (Fig. 3 and Table 2).

AAV-ChR	Morphology	Number of wells	RR (ms)	EFP-DT	FPD tangent	FPD threshold	FPD tangent vs. threshold p-values
No	Standard	303	798.6 (314.3)	58.9 (21.6)	293.0 (47.5)	461.0 (82.1)	< 0.001
	Small Tamp	100	778.0 (202.2)	59.8 (17.9)	466.3 (170.6)	603.5 (174.2)	0.06
	Biphasic	27	839.1 (512.4)	108.5 (123.5)	602.9 (280.4)	736.1 (349.3)	0.96
Yes	Standard	55	995.4 (4.99)	26.4 (14.7)	283.7 (54.2)	442.9 (109.2)	< 0.001
	Small Tamp	21	993.7 (4.93)	29.8 (28.1)	542.8(182.2)	690.2 (185.9)	0.01
	Biphasic	2	994.7 (6.65)	45.2 (26.7)	369.9 (120.3)	690.3 (199.1)	0.22
AAV-ChR (Yes vs. No) p-values	Standard	NA	< 0.001	< 0.001	0.32	0.31	NA
	Small Tamp		< 0.001	< 0.001	0.16	0.02	
	Biphasic		0.42	0.91	0.14	0.69	

Table 1. Comparison of EFP parameters based on morphology & measurement method. The numbers represent mean (standard deviation).: AAV: adeno-associated virus; EFP: extracellular field potential, iPSC-CM: induced pluripotent stem-cell derived cardiomyocyte, CRISPR: clustered regularly interspaced short palindromic repeats; FPD: Field Potential Duration; RR: time between two successive waves from the start of DT. EFPs are classified into three morphologies: Standard, Small Amplitude (Small Tamp), and Biphasic. The parameters measured include RR interval (ms), EFP-DT (ms), FPD tangent (ms), and FPD threshold (ms). The data compare wells treated with AAV-ChR (Yes) to untreated controls (No), with p-values provided for statistical significance. Standard morphology exhibits the highest number of wells and the most consistent measurements across all parameters.
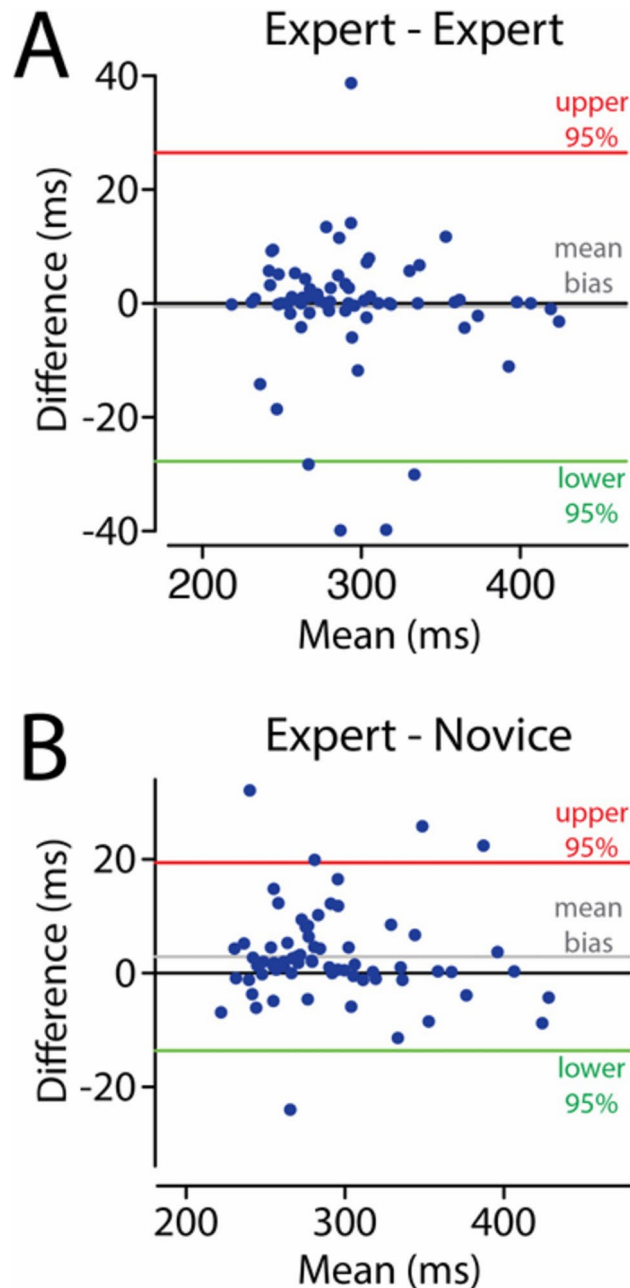
Fig. 3. Comparison in FPD (ms) between Intra and Inter Reader. (**A**) Difference in FPD (ms) between intra-reader (expert-expert). (**B**) Difference in FPD (ms) between inter-reader (expert-novice). *Each datapoint represents spontaneously beating cells.

The correlation coefficient for inter-reader FPD measurements (tangent method) ranged from $r = 0.93$ to 1.00 (Table 3). FPD (tangent method) values were shorter in paced EFPs compared to spontaneous EFPs (283.7 ± 54.2 ms vs. 293.0 ± 47.5 ms, respectively), partly due to shorter DTs observed in paced EFPs (26.4 ± 14.7 ms) compared to spontaneous EFPs (58.9 ± 21.6 ms). Data on Bland–Altman plots and intraclass correlation coefficients for intra- and inter-reader reproducibility of FPDmax measurements using the threshold method are provided in Table 2.

To further assess cross-user consistency, three additional novice users were recruited: Novice A & B, with less than one year of experience in research; Novice C, with less than two years of experience in research. A total of 96 raw traces were given to analyze after reading the manuscript, reviewing EFPA GitHub instructions, and completing a 10-min training session (Figure S7). After application of quality control criteria, 45 total comparisons remained. Inter-reader FPDmax were highly consistent within novice groups (95% CI of -6.7 to $+6.7$ ms, Bland–Altman).

AAV-ChR	Morphology	Number of wells analyzed	FPD tangent consistency intra-reader (ms)	FPD tangent consistency inter-reader (ms)	FPD threshold consistency intra-reader (ms)	FPD threshold consistency inter-reader (ms)
No	Standard	68	-0.6 (11.2)	2.3(13.1)	-3.6(21.3)	3.9(23.4)
	Small Tamp	24	-2.0 (15.9)	-2.8 (47.1)	-9.1(25.5)	19.5(28.8)
	Biphasic	8	-18.7 (64.9)	-39.2 (104.5)	-32.9(39.6)	30.6(126.1)
Yes	Standard	73	-0.7 (8.6)	1.0 (7.3)	-0.1(5.6)	-0.2(10.8)
	Small Tamp	25	-5.2 (36.0)	-6.5 (43.3)	0.7(5.5)	-7.3(34.3)
	Biphasic	2	-2.4 (27.4)	8.5 (12.0)	-31.2(44.1)	-31.2(44.1)

Table 2. Comparison of EFP consistency based on inter and intra reader and measurement method. ChR: channelrhodopsin. Morphological classifications include Standard, Small Amplitude (Small Tamp), and Biphasic. The table highlights the consistency of FPD tangent and FPD threshold parameters within intra-reader and inter-reader analyses. Consistent values are observed across Standard morphologies, while Small Tamp and Biphasic morphologies exhibit higher variability, particularly in inter-reader assessments.

AAV-ChR	Morphology	Number of wells analyzed	Intra Correlation Coefficients FPD tangent consistency	Inter Correlation Coefficients FPD tangent consistency	Intra Correlation Coefficients FPD threshold consistency	Inter Correlation Coefficients FPD threshold consistency
No	Standard	68	0.97	0.96	0.97	0.95
	Small Tamp	24	1.00	0.98	0.99	0.98
	Biphasic	8	0.97	0.93	0.99	0.96
Yes	Standard	73	0.99	0.99	1.00	1.00
	Small Tamp	25	0.98	0.98	1.00	0.99
	Biphasic	2	1.00	1.00	1.00	1.00

Table 3. Comparison of FPD consistency based on inter and intra reader and measurement method. Intra: collected values from one reader; Inter: differences between collected values from different readers. Coefficients of correlation between and across readers for FPD tangent and threshold consistency across various morphologies and AAV-ChR conditions, with the number of wells investigated.

Application to drug response and disease

We analyzed the EFP-Analyzer tool's ability to identify changes to EFP pattern/landmarks in response to drugs and in the case of individuals with disease through FPDmax analysis. As a key in-vitro correlate of arrythmia due to QT prolongation resulting from variants or drug exposure, FPDmax was selected as the representative parameter for intra- and inter-reader reproducibility analysis. Future analysis of other parameters quantified by the EFPA software, such as DT or beat rate, may further address the holistic reproducibility of EFPA. We first analyzed the action potential-prolonging drug moxifloxacin. We successfully detected an increase in FPDmax in response to increasing doses of moxifloxacin, with 119 ± 9.9 ms prolongation at 100 uM (Fig. 4). Next, we re-analyzed a previously published cell line carrying a pathogenic Long QT Type 8 *CACNA1C* variant N639T. Consistent with the previous study, relative to isogenic controls (non-CRIPSR edited) the mutation positive cell line had FPDmax prolongation in optically paced cells, (n = 15 cells/line, p < 0.002, two-tailed t test, Fig. 4).

Discussion
Summary

The EFP-Analyzer (EFPA) aims to streamline cardiac disease modeling. We showed consistency in measurements in interpretation of beats and landmarks across 22 patient lines with 358 traces. We were able to reliably detect pharmacological (moxifloxacin) and pathological alterations (CACNA1C N639T) from functional signatures. We further established strong inter-reader correlation coefficients (r = 0.93–1.00) for FPD measurements and observed good agreement in Bland–Altman plots, with mean difference values reflecting high consistency between readers. This technology not only allows for high-quality data capture, but it also ensures replicability across multiple users and studies[10], representing a significant advancement in integrating iPSC-CMs in drug screening paradigm. EFPA's versatility and convenience of use are critical for promoting wider adoption in academic and pharmaceutical research, notably in improving the efficiency, accuracy, and accessibility of EFP measurements.

The EFP analyzer is a fast, consistent tool for data analysis

The data derived from EFPA is robust and consistent between multiple observers. Analysis of 9 replicate sweeps in a 96-well plate took 12 ± 3 min, with a mean difference between observers of 20–25 ms for unpaced and 8–12 ms for paced cells. This approaches the robustness achievable in an ECG's QTc, typically considered to be around 12 ms[14]. Uniform synchronous depolarization of an entire well using optical pacing may result in a more
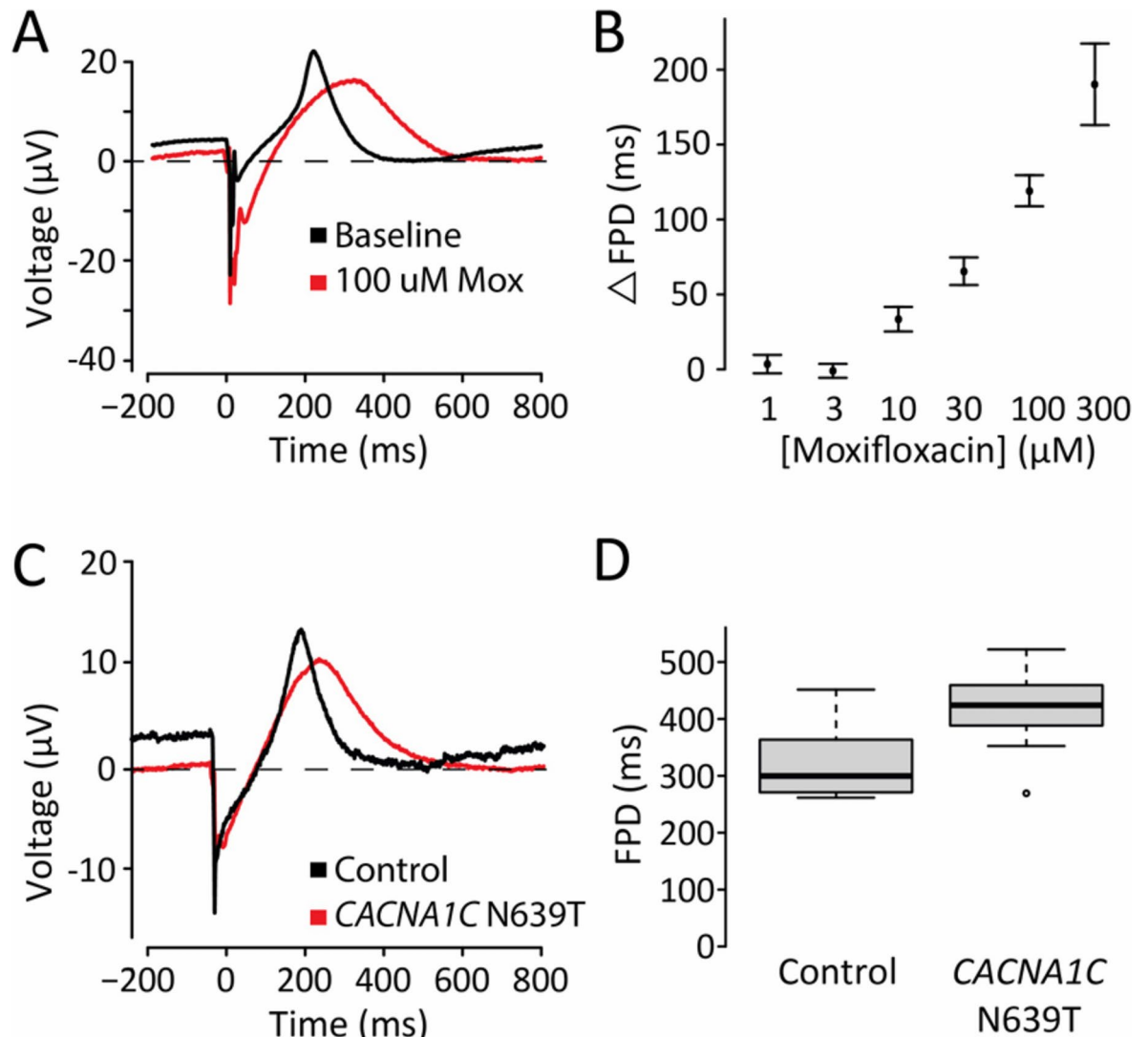
Fig. 4. FPD response in an exposure to IKr Blocker and CACNA1C N639T. (**A**) Representative EFP trace from an example cell treated with 100uM Moxifloxacin. (**B**) As the dose of moxifloxacin increased, the change in QT was measured. Each measurement represents n = 11 traces. (**C**) Representative EFP trace from an example N639T mutation positive cell. (**D**) The mutation positive cell line had prolongation in optically paced cells, (n = 15) cells expressing CACNA1C N639T mutation exhibit a prolonged FPD compared to control cells (n = 19).

repeatable (and 25 ms shorter) FPDmax than spontaneous cell activation, which requires the signal to spread throughout the well from a point of activation. Optical pacing provides precise and controlled stimulation, whereas spontaneous beating reflects intrinsic cell behavior but may exhibit variability and inconsistency. Limitations include the need for optogenetic modifications in optical pacing and the lack of consistent pacing rates in spontaneous conditions, which can affect reproducibility and comparability across studies[14].

Recommendations for improving EFP quality/robustness

We observed a range of EFP morphologies, which we termed standard, low amplitude, and biphasic. We found that according to a variety of metrics, low amplitude and biphasic EFPs generated non-robust data, leading to highly variable, inconsistently measured values. We therefore recommend that these classes be removed. The tangent approach also improved the robustness of the EFPs according to these metrics. We note that these parameters were optimized on EFPs generated from one device, the Nanion CardioExcyte 96. Alternative cardiac screening instruments may differ in system defaults such as sampling rates, leading to potential differences in results.

For ECG analysis, a return to baseline of the QT is commonly used with multiple input convergence. However, in some cases the T wave has an extended unclear return to baseline particularly the lower the T peak is in term of amplitude, and a tangent method (drawn at the steepest point) yields more robust FPD measurements[20]. We observed that some EFPs had long extended repolarization waves, analogous to T waves in the ECG. Thus, we

employ the tangent method and observed a decrease in the standard deviation of the tangent and threshold method across many wells, which suggests both approaches are accurate/repeatable; we similarly observed more robust measurements when comparing across multiple observers.

Comparison to other methods/tools

The CardioExcyte 96 has well been defined by several groups in high throughput genomic and pharmacological investigations and has since proven to be invaluable across disciplines[3,19,21–23]. While built-in tools like LabChart can calculate intervals, it has notable limitations when analyzing iPSC-CM data, particularly in handling variability such as spontaneous beating, immature electrophysiological profiles, and irregular patterns. These limitations often require significant manual intervention and may lead to inaccuracies in detecting key landmarks. In comparison, the EFP Analyzer offers greater flexibility and enhanced capabilities, such as the tangent method, manual beat adjustment, and persistent data storage. It standardizes the baseline start for each complex and allows additional analyses, like calculating T-Amp, improving precision and accuracy. Unlike LabChart, which struggles with inconsistent traces, the EFP Analyzer's semi-automated approach often identifies landmarks correctly without adjustments, though manual optimization remains possible for more complex patterns. Additionally, the EFP Analyzer functions as an effective data organizer, simplifying analysis, review, and editing processes, which is particularly beneficial for collaboration among researchers.

The following EFP Parameters can be generated from the EFP Analyzer: (1) Beat Rate, a measurement of the number of beats per unit of time that serves as a basic indicator of cardiac activity (2) Depolarization Time (DT), which indicates the time interval of the depolarization phase, (3) T-Amplitude (T-amp), which quantifies the amplitude of the T wave to provide insights into repolarization wave features. (4) Field Potential Duration Maximum (FPD max), essential parameter for evaluating repolarization and drug effects.

Users can manually modify important landmarks in the EFP Analyzer to enhance the accuracy of their analyses. These include T-Start, an adjustable start point for the repolarization phase that facilitates accurate FPD measurements; T-Peak, which allows precise marking of the T wave's peak for assessing T-amp and repolarization dynamics; Baselines, which can be set and adjusted to ensure accurate measurements; and QRS Start and End, editable landmarks for the depolarization phase crucial for defining DT and FPD.

Limitations

iPSC-derived cardiomyocytes (iPSC-CMs) have an immature phenotype, including simpler electrophysiological characteristics, weaker contractility, and shorter action potentials relative to adult human cardiomyocytes. The inability to fully mature, remaining in an embryonic or fetal-like state, is a key limitation for most iPSC-derived cell types[24,25]. While advancements have been made for iPSC-CMs, further optimization would increase the predictive accuracy of disease and drug modeling.

Additional EFP parameters such as conduction velocity, refractory period, and spatial dispersion of electrical signals, could be investigated to provide deeper insights into the capture of electrophysiological properties of tissues and their responses to various stimuli or drugs. Furthermore, examining the effects of mutations in key ion channels, such as CACNA1C and KCNQ1, using iPSC-derived models could reveal how a plethora of genetic alterations impact cardiac electrophysiology to further review the consistency of this tool across cell-lines and disease conditions. Further studies using different cellular modalities, primary cells, 3D culture, and co-culture, may further understanding of the limitations and potentials of EFPA.

The ability of this software to analyze EFP repolarization wave characteristics was demonstrated in our investigation. Even though T peak amplitude and T peak T_{end} are important clinical metrics, we did not test the capability to analyze these characteristics[14]. Furthermore, we did not study HR dependence of field potential duration. We observed a RT-peak amplitude decrease with moxifloxacin incubation, which calls for further investigation. Additionally, this method has also been compatible with *CACNA1C* N639T, a cell line with a congenital Long QT syndrome type 8. This program was customized for Nanion CardioExcyte 96 (Nanion Technologies, Germany) and datasets with fundamentally similar EFP shapes. Data processing devices with differing EFP characteristic output, such as MEAs, may pose as a limitation. Further compatibility testing and hardware configurations would identify the software's maximum analytical capabilities. Users are encouraged to test its limits, submit feedback, and contribute suggestions for improvement.

Declaration

Data availability

All data, script, and directions used for this manuscript can be found on https://github.com/kroncke-lab/EFPA.

References

1. Takahashi, K. & Yamanaka, S. Induction of pluripotent stem cells from mouse embryonic and adult fibroblast cultures by defined factors. *Cell* https://doi.org/10.1016/j.cell.2006.07.024 (2006).
2. Shi, Y., Inoue, H., Wu, J. C. & Yamanaka, S. Induced pluripotent stem cell technology: A decade of progress. *Nat. Rev. Drug Discov.* https://doi.org/10.1038/nrd.2016.245 (2017).
3. Denning, C. et al. Cardiomyocytes from human pluripotent stem cells: From laboratory curiosity to industrial biomedical platform. *Biochim. Biophys. Acta Mol. Cell Res.* https://doi.org/10.1016/j.bbamcr.2015.10.014 (2016).
4. Vicente, J. et al. Mechanistic model-informed proarrhythmic risk assessment of drugs: Review of the "CiPA" initiative and design of a prospective clinical validation study. *Clin. Pharmacol. Ther.* https://doi.org/10.1002/cpt.896 (2018).

5. Millard, D. et al. Cross-site reliability of human induced pluripotent stem cell-derived cardiomyocyte based safety assays using microelectrode arrays: Results from a blinded cipa pilot study. *Toxicol. Sci.* https://doi.org/10.1093/toxsci/kfy110 (2018).
6. Laverty, H. G. et al. How can we improve our understanding of cardiovascular safety liabilities to develop safer medicines?. *Brit. J. Pharmacol.* https://doi.org/10.1111/j.1476-5381.2011.01255.x (2011).
7. Cavero, I. et al. Comprehensive in vitro proarrhythmia assay (CiPA): Pending issues for successful validation and implementation. *J. Pharmacol. Toxicol. Methods* https://doi.org/10.1016/j.vascn.2016.05.012 (2016).
8. Stillitano, F. et al. Modeling susceptibility to drug-induced long QT with a panel of subject-specific induced pluripotent stem cells. *Elife* https://doi.org/10.7554/eLife.19406 (2017).
9. Garg, P. et al. Genome editing of induced pluripotent stem cells to decipher cardiac channelopathy variant. *J. Am. Coll. Cardiol.* https://doi.org/10.1016/j.jacc.2018.04.041 (2018).
10. Chavali, N. V. et al. Patient-independent human induced pluripotent stem cell model: A new tool for rapid determination of genetic variant pathogenicity in long QT syndrome. *Heart Rhythm* https://doi.org/10.1016/j.hrthm.2019.04.031 (2019).
11. Dwenger, M. et al. Chronic optical pacing conditioning of h-iPSC engineered cardiac tissues. *J. Tissue Eng.* https://doi.org/10.1177/2041731419841748 (2019).
12. Parikh, S. S. et al. Thyroid and glucocorticoid hormones promote functional t-tubule development in human-induced pluripotent stem cell-derived cardiomyocytes. *Circ. Res.* https://doi.org/10.1161/CIRCRESAHA.117.311920 (2017).
13. Halbach, M. D., Egert, U., Hescheler, J. & Banach, K. Estimation of action potential changes from field potential recordings in multicellular mouse cardiac myocyte cultures. *Cell. Physiol. Biochem.* https://doi.org/10.1159/000074542 (2003).
14. Saqué, V. et al. Fast, accurate and easy-to-teach QT interval assessment: The triplicate concatenation method. *Arch. Cardiovasc. Dis.* https://doi.org/10.1016/j.acvd.2016.12.011 (2017).
15. Patejdl, R., Gromann, A., Bänsch, D. & Noack, T. Effects of ajmaline on contraction patterns of isolated rat gastric antrum and portal vein smooth muscle strips and on neurogenic relaxations of gastric fundus. *Pflugers Arch.* https://doi.org/10.1007/s00424-019-02279-y (2019).
16. Printemps, R., Guilbot, S., Didier, H., Nalin, R. & Le Grand, B. The cardiotoxic effect of roundup® is not induced by glyphosate: A non-specific blockade of human CaV1.2 channels. *Cardiovasc. Toxicol.* https://doi.org/10.1007/s12012-022-09749-3 (2022).
17. Wei, X. et al. Hypoglycemia-Exacerbated mitochondrial connexin 43 accumulation aggravates cardiac dysfunction in diabetic cardiomyopathy. *Front. Cardiovasc. Med.* https://doi.org/10.3389/fcvm.2022.800185 (2022).
18. Alexandrou, A. J. et al. Mechanism of hERG K + channel blockade by the fluoroquinolone antibiotic moxifloxacin. *Br. J. Pharmacol.* https://doi.org/10.1038/sj.bjp.0706678 (2006).
19. Clements, M. & Thomas, N. High-throughput multi-parameter profiling of electrophysiological drug effects in human embryonic stem cell derived cardiomyocytes using multi-electrode arrays. *Toxicol. Sci.* https://doi.org/10.1093/toxsci/kfu084 (2014).
20. Lester, R. M., Paglialunga, S. & Johnson, I. A. QT assessment in early drug development: The long and the short of it. *Int. J. Mol. Sci.* https://doi.org/10.3390/ijms20061324 (2019).
21. Wang, Y. et al. Single-cell analysis of murine fibroblasts identifies neonatal to adult switching that regulates cardiomyocyte maturation. *Nat. Commun.* https://doi.org/10.1038/s41467-020-16204-w (2020).
22. del Álamo, J. C. et al. High throughput physiological screening of iPSC-derived cardiomyocytes for drug development. *Biochim. Biophys. Acta Mol. Cell Res.* https://doi.org/10.1016/j.bbamcr.2016.03.003 (2016).
23. Wang, H. et al. Three tyrosine kinase inhibitors cause cardiotoxicity by inducing endoplasmic reticulum stress and inflammation in cardiomyocytes. *BMC Med.* https://doi.org/10.1186/s12916-023-02838-2 (2023).
24. Pourrier, M. & Fedida, D. The emergence of human induced pluripotent stem cell-derived cardiomyocytes (hiPSC-CMs) as a platform to model arrhythmogenic diseases. *Int. J. Mol. Sci.* https://doi.org/10.3390/ijms21020657 (2020).
25. Kistamás, K. et al. Calcium handling defects and cardiac arrhythmia syndromes. *Front. Pharmacol.* **11**, 72 (2020).

Author contributions

A.S., N.P., J.S., A.M.G., and B.M.K. wrote the original manuscript; A.S., N.P., Y.W., M.B., D.M., L.V., S.W., M.K., K.D., W.M., M.Y., J.S., A.M.G., B.M.K, B.C.K., reviewed and edited the manuscript; A.S., N.P., J.S., A.M.G., B.M.K, B.C.K., designed the research; A.S., N.P., A.M.G., Y.W., M.B., L.V., S.W., M.K., M.Y., performed the research; A.S., N.P., J.S., A.M.G., B.M.K., K.D., D.W.M., analyzed the data.

Funding

Competing interests

The authors declare no competing interests.

Additional information

Supplementary Information The online version contains supplementary material available at https://doi.org/10.1038/s41598-025-88946-w.

Correspondence and requests for materials should be addressed to A.M.G. or B.M.K.

Reprints and permissions information is available at www.nature.com/reprints.

Publisher's note Springer Nature remains neutral with regard to jurisdictional claims in published maps and institutional affiliations.